NUCLEAR INSTRUMENTS AND METHODS 71 (1969) 163–169; © NORTH-HOLLAND PUBLISHING CO.

GAMMA RAY IMAGE CHARACTERISTICS IN SODIUM IODIDE SLABS

G. F. KNOLL

The University of Michigan, Ann Arbor, Michigan, U.S.A.

Received 7 January 1969

A Monte Carlo calculation has been made of the effects of detector scattering on the gamma ray imaging properties of sodium iodide slabs. All interactions within the detector were assumed to contribute to the image. A detailed accounting was kept of the radial distribution away from the point of incidence of both the number of interactions and the deposited energy. Data are presented for slabs of thickness ranging from $\frac{1}{8}''$ to $2''$ and over the energy interval from 140 – 999 keV.

1. Introduction

A number of devices have recently been developed for the purpose of visualizing the spatial distribution of gamma ray emitting radioisotopes for medical and other applications. Several of these gamma ray cameras are based on the principle of image formation in a slab shaped scintillation crystal through parallel hole or pinhole collimators[1-5]). The spatial resolution of this type of imaging is determined by a number of factors, including the geometry of the collimation, scattering of the gamma ray photons before reaching the crystal, and scattering within the crystal itself. The last of these effects is the subject of the study reported in this paper.

The light distribution generated in the scintillation crystal would be an accurate reproduction of the gamma ray distribution transmitted by the collimator if all interactions in the crystal were simple photoelectric absorption events. Since there will always be some degree of Compton scattering as well, multiple interactions from a single incident gamma ray photon will lead to some energy deposition away from the initial point of incidence and a corresponding loss in image resolution and contrast. Any pulse height selection process based on the total light yield from the crystal cannot eliminate this degradation of image quality since the summed light output from multiple interactions will often be the same as that from a single photoabsorption. The effects of multiple scattering in the crystal will, in general, become more pronounced as the incident gamma ray energy increases or the crystal slab thickness is made larger.

The magnitude of resolution loss through multiple interactions has previously been investigated by Anger and Davis[6]) through a Monte Carlo simulation of various energy gamma ray photons in sodium iodide. The emphasis in this previous investigation was the spread in the position of the centroid of light generated in multiple interactions, since the particular gamma ray camera of interest in that work records the centroid position whenever multiple events take place. Other types of cameras, such as those employing electronic image intensification[3-5,7,8]), record each scintillation individually, regardless of whether more than one originate from the same incident gamma ray photon. The Monte Carlo calculation reported here has been made to re-examine the effects of crystal scattering, considering each interaction separately and sorting to provide information on a variety of effects influencing image resolution and efficiency. No pulse height selection is assumed, and data is presented on the distribution of both the number of gamma ray interactions as well as the energy deposited in the crystal. Assuming linearity of the scintillation response, the latter will also describe the spatial distribution of light emitted by the scintillation crystal for point illumination by gamma rays.

2. Calculations

The results presented in the following sections were derived through the use of two programs run on the University of Michigan IBM 7090 computer. The first of these, designated TRACK, generated individual gamma ray histories in an infinite medium of sodium iodide for six source energies ranging from 140 to 999 keV. The second program, called SORT, used the histories generated by TRACK as input data and sorted through each history imposing the geometry conditions corresponding to slabs of thickness from $\frac{1}{8}''$ to $2''$.

3. TRACK program

Individual histories are generated by starting each gamma ray photon at coordinates (0, 0, 0) and with the initial velocity vector oriented along the Z-axis. The initial free path length is sampled using Monte Carlo techniques with knowledge of the total inter-

action cross section at the source energy. At the first interaction, the ratio of Compton to photoelectric cross sections is used to randomly select one of the two interaction processes. No biasing techniques are used. If the initial event sampled is a photoelectric absorption, the history is terminated and the output routine initiated. If the first event is instead a Compton scattering, a new photon of degraded energy is generated whose direction is chosen randomly by sampling the Klein-Nishina cross section using the rejection method of Kahn[9]). The deposited energy is recorded in memory corresponding to the particular angle of scatter which has been selected. The degraded photon is tracked further through the infinite sodium iodide medium and the position of its next interaction again sampled using the total cross section at the degraded photon energy. At each interaction, the ratio of Compton to photoelectric cross sections is sampled to determine whether the history is terminated (photoelectric) or continued at a lower energy (Compton).

The TRACK program as written considers only photoelectric and Compton events, and the finite path length of secondary electrons is neglected. The cross section data was obtained from the compilations of Grodstein[10]) and McGinnies[11]) and are entered in the program as expansion coefficients applicable over discrete energy intervals from 10 to 1000 keV. Each history is continued until it terminates with a photoelectric absorption. The output routine then records the following information: the source energy, the number of interactions in the history, followed by the spatial coordinates and deposited energy for each interaction.

Some sorting was applied to the results of TRACK, including a simple count of the number of histories undergoing a given number of interactions (either scattering events or photoabsorption). The results are plotted in fig. 1 and illustrate the increased incidence of multiple scattering with increasing energy.

4. SORT program

The 1000 infinite medium histories generated by TRACK at each energy served as input data for the SORT program, which simulates the geometry of a slab of arbitrary thickness and radius of $4\frac{1}{2}''$. The specific choice of radius has little effect on the examples shown here, since virtually no photons escape in the radial direction.

The data of the first history are read and the position of the first interaction noted. A test is then made to determine whether this position lies within a slab defined by the planes $Z = 0$ and $Z = T$. If the coordinates lie outside the dimensions so defined, the history is recorded as one in which the incident gamma ray has passed through the slab without interacting. If the interaction is found to lie within the boundaries, the coordinates and deposited energy at the interaction are recorded and the coordinates of

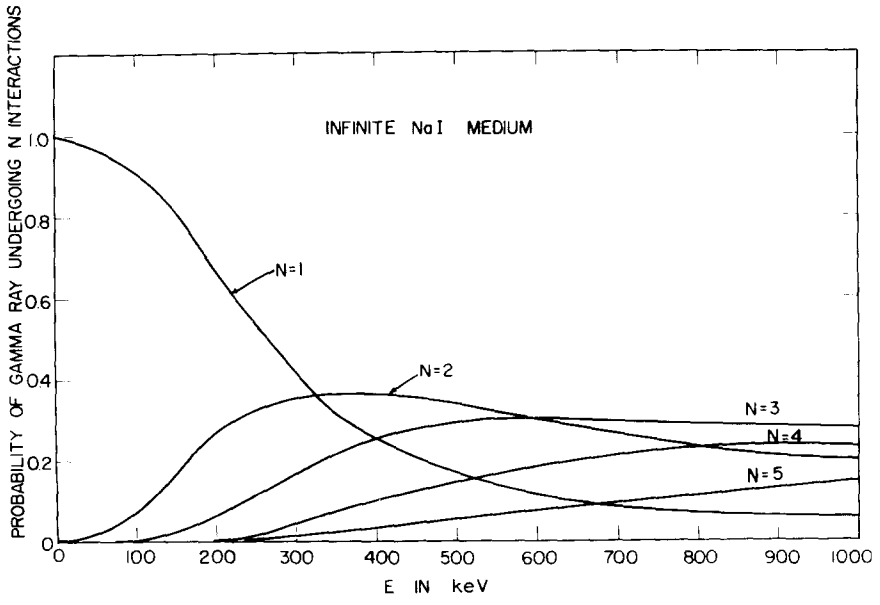

Fig. 1. Probability of gamma ray with initial energy E undergoing N interactions including final photoelectric absorption.

the next interaction inspected in a similar fashion. At each interaction beyond the first, a further test is made to determine whether the X and Y coordinates correspond to a radius greater than the crystal radius. This process is repeated for successive interactions of the history until either the photon is found to escape from the slab or until the final photoelectric interaction has occurred. Each history is sorted in a similar fashion and categorized in a number of ways to be described in the next section.

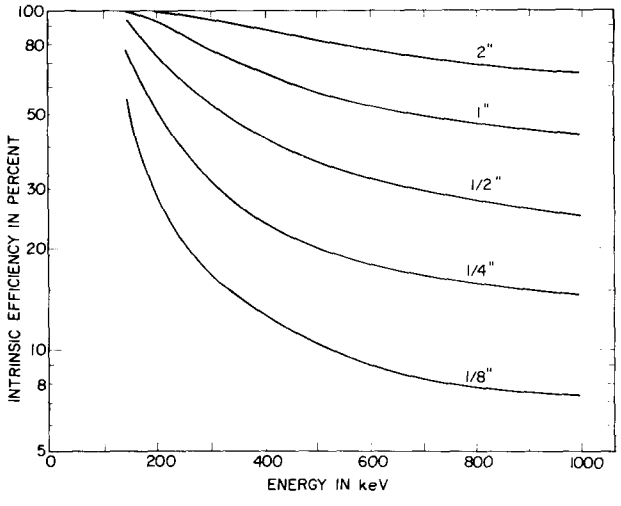

Fig. 2. Intrinsic efficiency for sodium iodide of thickness from $\frac{1}{8}'' - 2''$.

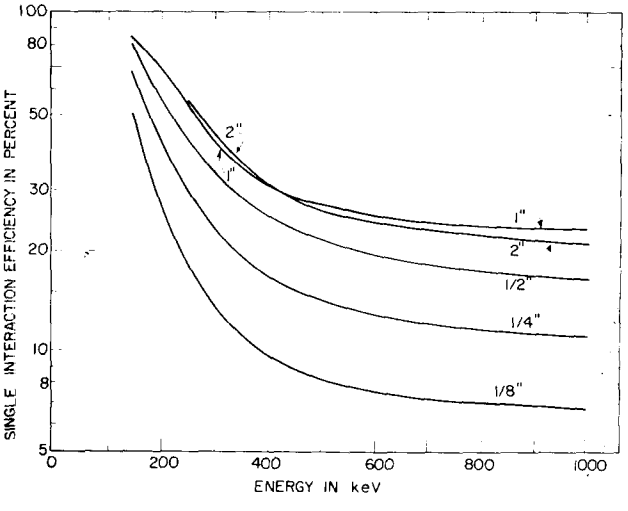

Fig. 3. Single interaction efficiency for sodium iodide of thickness from $\frac{1}{8}'' - 2''$.

The histories were sorted for slab thicknesses of $\frac{1}{8}''$, $\frac{1}{4}''$, $\frac{1}{2}''$, $1''$ and $2''$. Some of the results of interest in image formation are shown in figs. 2–13.

5. Results

Some of the properties calculated in this work are directly comparable with those of Anger and Davis[6]). Table 1 lists those which can be compared at an energy of 511 keV. The results are consistent to within statistical errors, and serve to verify that the computer programs have proceeded as expected.

TABLE 1

Comparison of present results with those of Anger and Davis[6]) at 511 keV.

Thickness:		$\frac{1}{8}''$	$\frac{1}{4}''$	$\frac{1}{2}''$	$1''$	$2''$
		(%)	(%)	(%)	(%)	(%)
Intrinsic efficiency	Present	10.2	19.9	35.4	57.8	82.6
	ref. [6])	10.2	19.3	34.9	57.6	82.0
Probability of history with initial photo-interaction	Present	1.2	3.3	6.2	9.2	13.1
	ref. [6])	1.6	3.1	5.6	9.2	13.1
Probability of Compton (single or multiple) and escape	Present	7.1	12.3	17.6	21.8	18.0
	ref. [6])	7.1	12.2	17.9	21.1	17.5
Probability of Compton (single or multiple) followed by photo-absorption	Present	1.9	4.2	11.7	26.8	51.5
	ref. [6])	1.4	4.0	11.4	27.3	51.4
Probability of full energy absorption	Present	3.1	7.6	17.9	36.0	64.6
	ref. [6])	3.0	7.1	16.9	36.5	64.5

Figs. 2 and 3 show the variation with energy of two quantities related to the detection efficiency of the slab. Fig. 2 displays the intrinsic efficiency, or probability of *at least one* interaction, which can also be calculated analytically from the cross section data. This quantity has often been used as a guide in choosing crystal thickness for a particular energy. Of more direct interest in image formation, however, is the probability that *only one* interaction (Compton or photo-absorption) takes place, since additional interactions occur away from the point of incidence and detract from the image. This quantity is plotted in

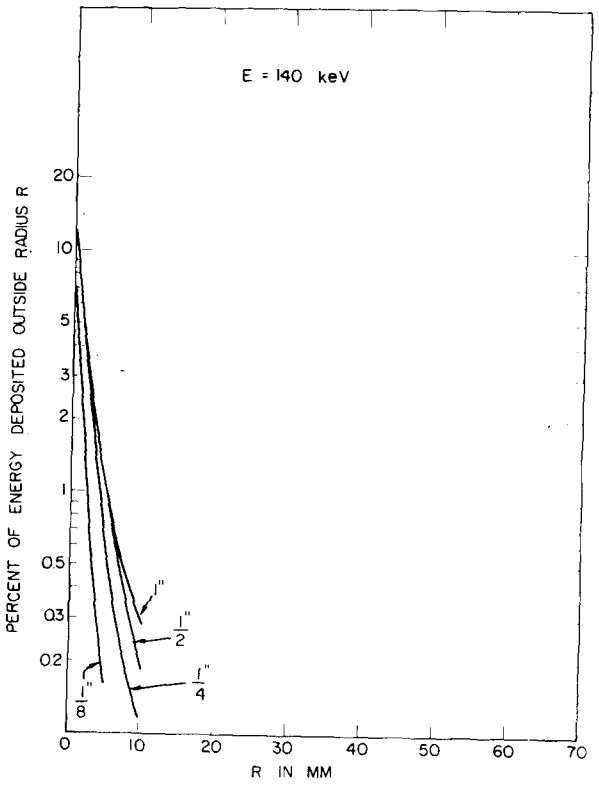

Fig. 4. This and the following five figures give the radial distribution of deposited energy for incident gamma rays of energy E. The case of $E = 140$ keV is shown here for the thicknesses of sodium iodide indicated on the plot.

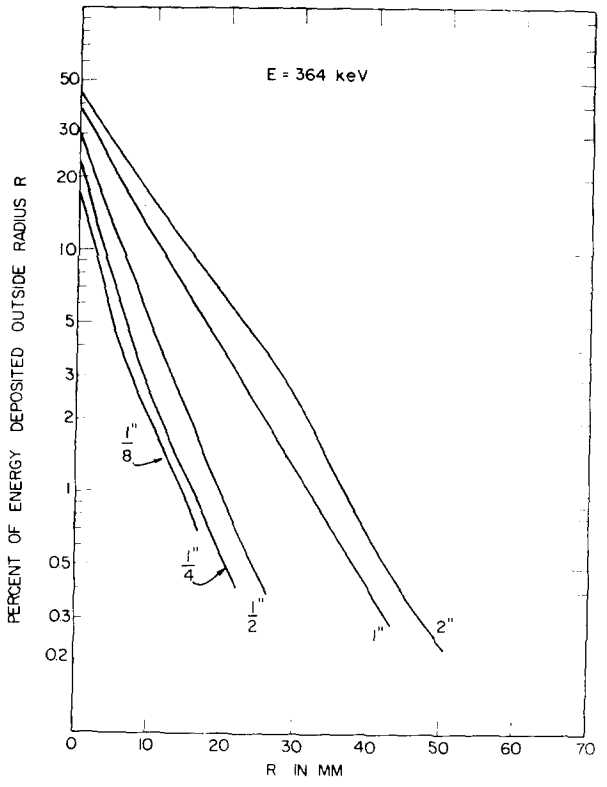

Fig. 6. Radial distribution of deposited energy for 364 keV gamma rays.

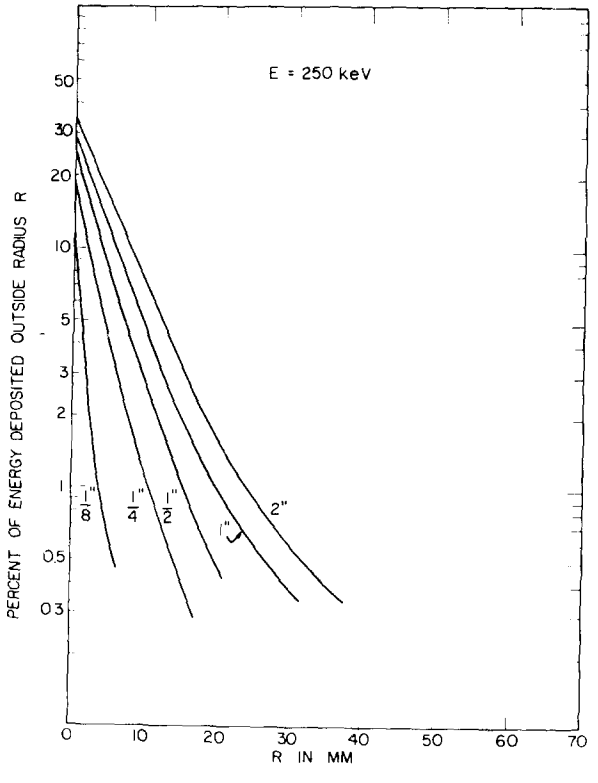

Fig. 5. Radial distribution of deposited energy for 250 keV

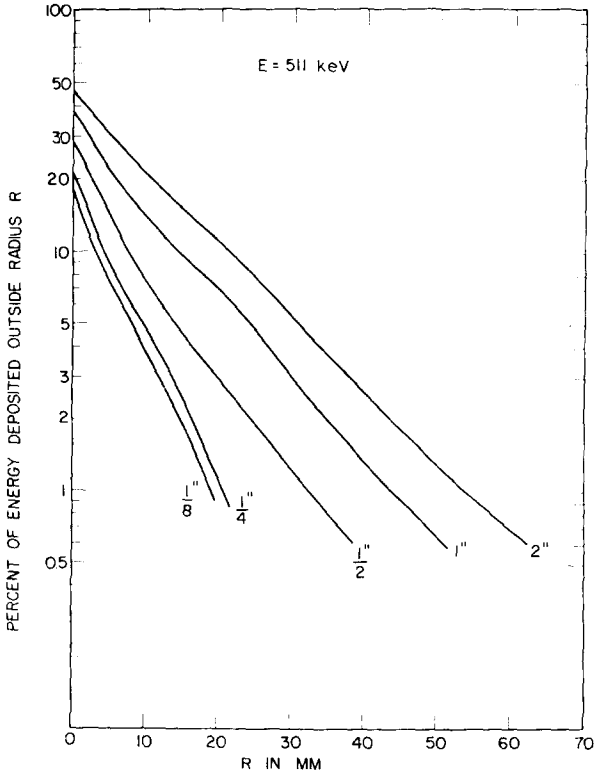

Fig. 7. Radial distribution of deposited energy for 511 keV

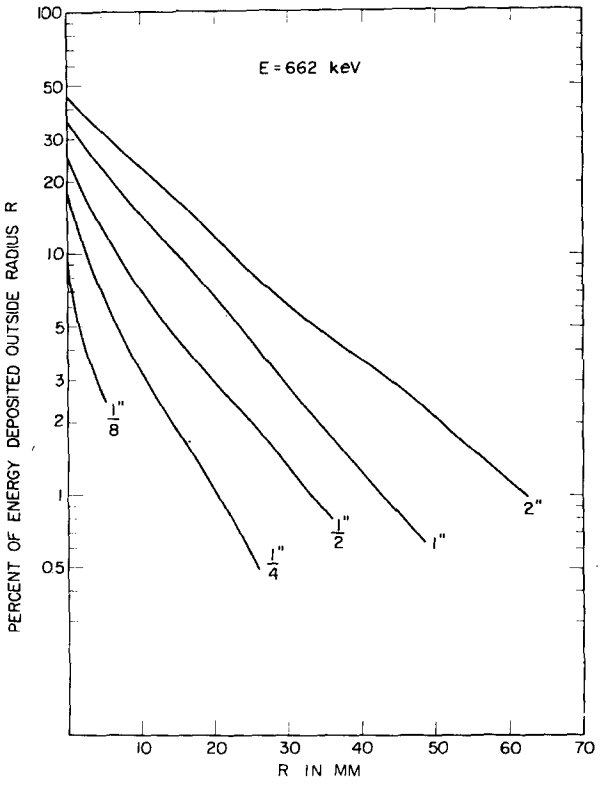

Fig. 8. Radial distribution of deposited energy for 662 keV gamma rays.

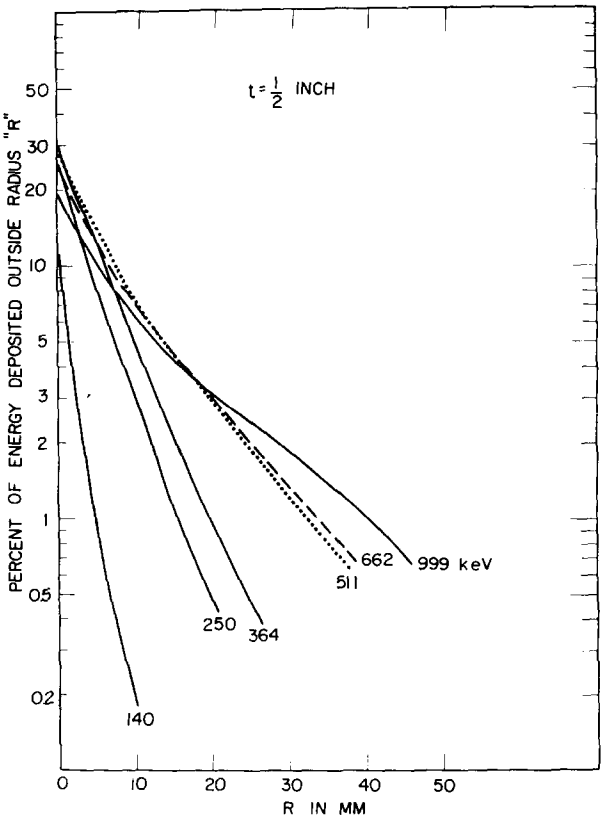

Fig. 10. Radial distribution of deposited energy for a $\frac{1}{2}''$ sodium iodide slab. Incident gamma ray energies are shown on the plot.

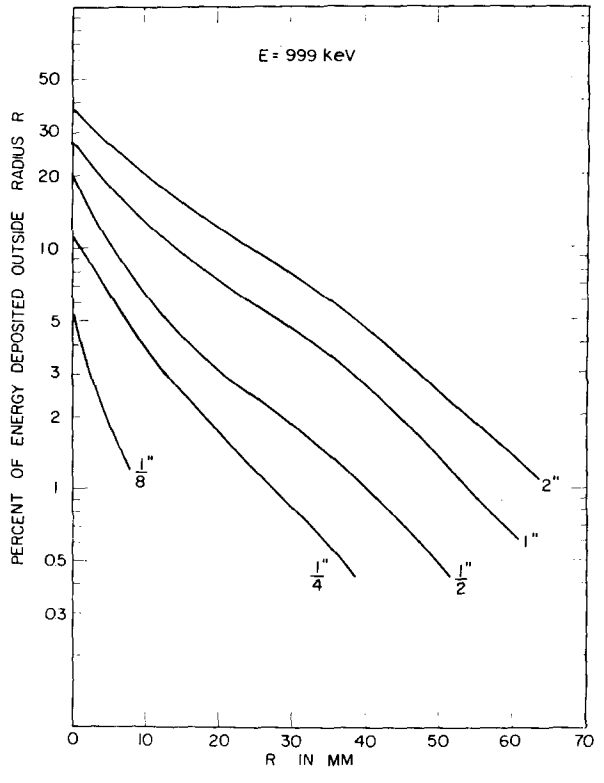

Fig. 9. Radial distribution of deposited energy for 999 keV

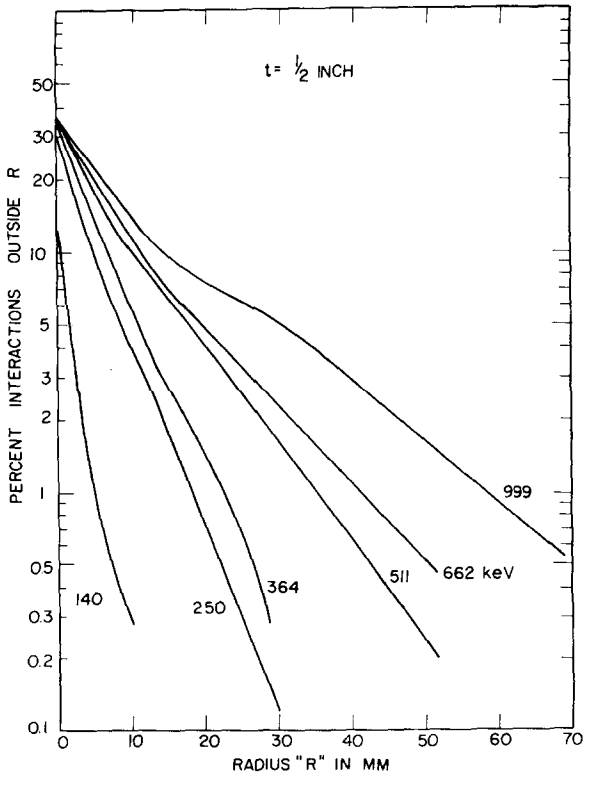

Fig. 11. Radial distribution of the total number of all types of

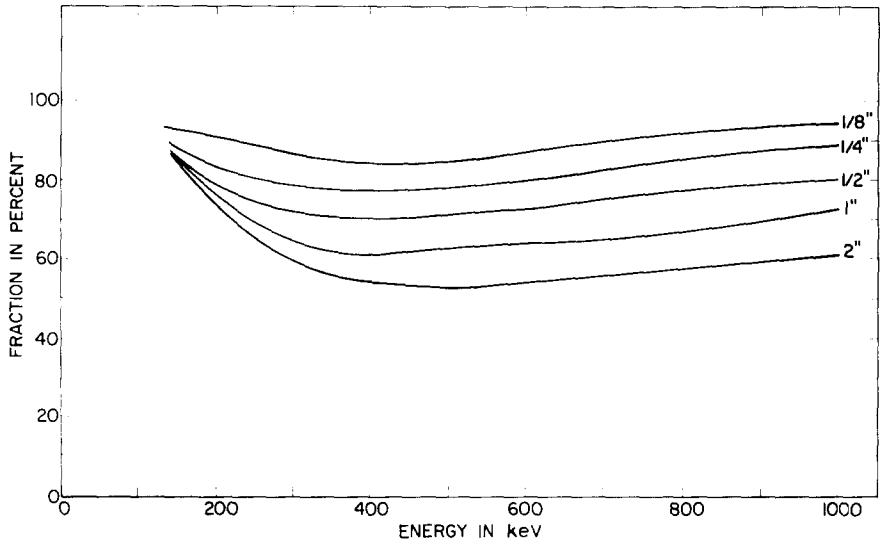

Fig. 12. The fraction of all energy deposited in the slab which is deposited at the point of incidence. Slab thickness is shown as a parameter.

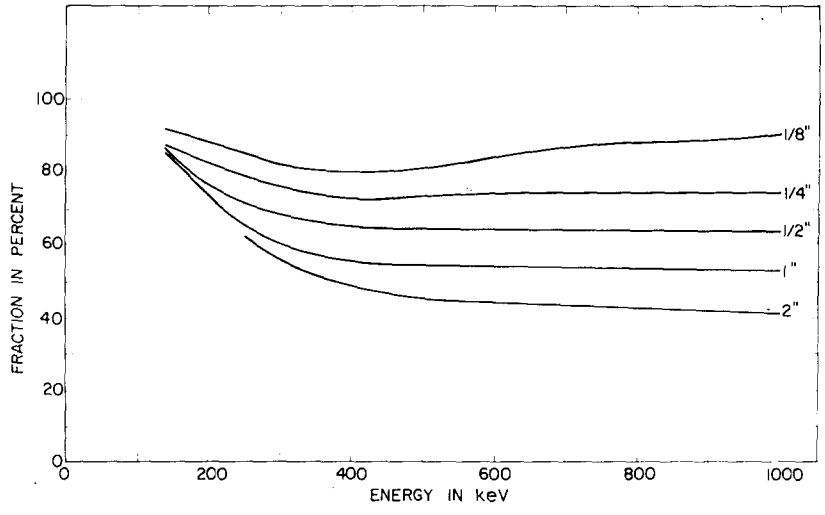

Fig. 13. The fraction of all types of interactions which occur at the point of incidence.

fig. 3 and shows a somewhat different variation, particularly for the larger thicknesses. The single interaction efficiency does not improve with larger thicknesses nearly as much as the intrinsic efficiency. In fact, above about 400 keV, a 2″ crystal will have a lower single interaction efficiency than a 1″ crystal, since the increased multiple scattering more than offsets the increased interaction probability.

Figs. 4–9 present data of primary importance in image resolution. Each of these plots shows the fraction of all energy deposited in the slab that is deposited *outside* the radius given along the abscissa. The value at $R = 0$ represents the fraction of deposited energy (or emitted light) that occurs at the point of incidence. The radius R in all cases is defined as the X-Y-plane projected radius, assuming the incident gamma ray to be along the Z-axis or center axis of the crystal. The generally increasing effects of multiple scattering with thickness and energy are illustrated by this series of plots.

The same data are also shown in fig. 10, but in this case collecting all data for a single thickness ($\frac{1}{2}$″). Most noticeable changes are seen to take place at the lower energies. Fig. 11 presents, for comparison, the

same type of plot for the fraction of all interactions, rather than total deposited energy. Since the general trends of these two plots are similar, it is apparent that no strong correlation exists between radial distance and average energy per interaction.

The other parameters of interest in image resolution appear in figs. 12 and 13. These plots show the fraction of deposited energy and total interactions which occur at the point of incidence as a function of incident energy. All the curves of fig. 12 show a broad minimum between 400 and 500 keV, indicating a somewhat surprising reversal in the image degradation effects with increasing energy above this point. The physical explanation for this behavior lies in the greater trend toward forward scattering events followed by escape of the scattered photon. The same general trend is also shown in fig. 13 for the fraction of interactions, although definite minima are present only for the thinner slabs.

The results of these calculations show that with respect to multiple crystal interactions the major deterioration in image resolution with increasing energy occurs up to about 400 keV. Beyond this energy, most effects remain relatively constant and some actually tend toward improved resolution at higher energies. The improvement in interaction efficiency with crystal thickness is less pronounced when one considers events which contribute constructively to image formation rather than all events, and must be weighed against the severely increased multiple scattering evidenced by all the properties listed in this study.

References

1) H. O. Anger, J. Nucl. Med. **5** (1964) 515.
2) P. M. Corry, Phys. Med. Biol. **11** (1966) 144.
3) R. J. Wilks and J. R. Mallard, Phys. Med. Biol. **12** (1967) 251.
4) M. Iio et al., IAEA Conf. *Medical radioisotope scintigraphy* (1968) paper SM-108/69.
5) F. D. Thomas et al., ibid., paper SM-108/96.
6) H. O. Anger and D. H. Davis, Rev. Sci. Instr. **35** (1964) 693.
7) M. M. Ter-Pogossian et al., Radiology **86** (1966) 463.
8) N. F. Moody, W. Paul and M. Joy, Trans. Am. Nucl. Soc. **11** (1968) 64.
9) H. Kahn, AECU-3259 (1954).
10) G. W. Grodstein, NBS-583 (1951).
11) R. T. McGinnies, Supplement to NBS-583 (1959).